Chapter 3

Ferromagnetic ZnO Nanowires for Spintronic Applications

Usha Philipose and Gopal Sapkota

Additional information is available at the end of the chapter

http://dx.doi.org/10.5772/52825

1. Introduction

Dilute Magnetic Semiconductors (DMS) are expected to be the main building blocks for the realization of semiconductor spin based electronics–spintronics. The giant magnetoresistance of these materials, i.e. large resistivity changes in response to an applied magnetic field, make them suitable for applications in magnetic sensors, magnetic random access memories and spintronic devices. DMS materials have been experimentally synthesized [1, 2] and theoretically modeled [3–5] for several years, focused on the transition metal (TM) doped group III-V and II-VI semiconductors. In order to develop spintronics as a practical technology, it is necessary to explore materials whose magnetic property can be controlled by changing either the external field or the carrier concentration. From an industrial point of view, it is essential to fabricate ferromagnetic DMS with Curie temperature (Tc) above room temperature and a ferromagnetism that is intrinsic, rather than due to the presence of dopant clusters. The synthesis of DMS as nanowires is particularly attractive for the fabrication of low dimensional, spin-based electronic and optoelectronic devices. Transition metals with partially filled d states (Sc, Ti, V, Cr, Mn, Fe, Co, Ni, and Cu) have been used as magnetic atoms in DMS. The electron spin of the partially filled d states are responsible for their magnetic behavior.

The field of spintronics gained prominence when $Ga_{1-x}Mn_xAs$ was found to be ferromagnetic up to 110 K [1] and up to 173 K with a Mn concentration of 6.8% [6]. Ferromagnetism in this DMS was explained in terms of carrier-mediated exchange coupling between the localized spins of the transition metal ions. It is based on the theory that doping GaAs with Mn introduces shallow acceptors and hence holes into the valence band of GaAs. These holes are anti-ferromagnetically coupled to the local Mn moments. Dietl calculated the Curie temperature of various DMS doped with Mn [3] and found this temperature to be proportional to the concentration of impurities and to the square root of the p-type charge

carrier concentration. Ferromagnetism has been predicted and confirmed in several III-V semiconductors doped with transition metal ions such as Mn, Cr, V, and Co. However, III-V semiconductors require complex processing steps and are expensive to synthesize. Moreover, obtaining T_c higher than room temperature poses a major challenge for development of III-V-based DMS.

The quest for materials with a high magnetic transition temperature continues and in this regard, TM doped II-VI semiconductors like ZnO has emerged as an attractive candidate as it is abundant, non-toxic and inexpensive to synthesize. ZnO is also a transparent, semiconducting oxide exhibiting piezoelectric and possibly ferromagnetic behavior. Dietl predicted room temperature ferromagnetism for 5% Mn in p-type wide band gap semiconductors like ZnO and GaN [3]. Sharma and coworkers reported room temperature ferromagnetism in Mn-doped ZnO thin films [2]. The author reported the first observation of room temperature ferromagnetism in Mn doped ZnO nanowires [7], and since then there have been works presenting evidence for intrinsic ferromagnetism in individual ZnO nanoparticles doped with TM ions [8]. However, recent experiments reveal inconsistent ferromagnetic properties for TM doped ZnO [9–13], leaving the real mechanism for ferromagnetism in ZnO unclear. There are several controversial and conflicting reports on TM doped ZnO; including claims that the magnetic signature arises from clustering, segregated phases [13, 14], or defect mediated ferromagnetic coupling [15, 16]. The controversy in understanding the origin of ferromagnetism in TM doped II-VI semiconductors like ZnO is because in II-VI materials, dopants like Mn behave as an isovalent impurity. When Mn^{2+} substitutes for Zn^{2+} in the ZnO lattice, it provides no additional carriers. Therefore, charge carriers would need to be provided by additional doping in order to render Mn-doped ZnO ferromagnetic. Based on the predictions by Dietl et al. [3], room temperature ferromagnetism is expected in Mn-doped ZnO in the presence of a fairly high hole concentration of $\approx 10^{20} cm^{-3}$. Such high hole concentrations seem rather unrealistic, especially, since it is difficult to achieve any reasonable concentration of holes in ZnO. The origin of experimentally observed ferromagnetism in TM doped II-VI semiconductors thus remains unclear. Kolesnik and coworkers [14] argue that the magnetic signature may arise from segregated phases of spinel oxides such as Mn_3O_4 that is ferromagnetic. Theoretical calculations predict that $Zn_{1-x}Mn_xO$ nanowires favor the ferromagnetic state if Zn vacancies are introduced, while they are anti-ferromagnetic unless additional carriers are incorporated [17].

In this chapter, we will review experimental results of observed room temperature ferromagnetism in TM doped II-VI semiconductors. Studies drawn primarily from the author's research along with similar experimental findings will be presented. The choice of nanowires (as opposed to thin films) for studying the origin of ferromagnetism in II-VI semiconductors is justified because they allow: (a) clean and smooth surfaces with no precipitates or attachments on the nanowire surface, and (b) a unique geometry for realizing spintronic devices with possible one dimensional charge transport.

2. Theory of ferromagnetism in ZnO based DMS

ZnO, a II-VI semiconductor, is a wide band gap (3.37 eV at room temperature) semi-conducting metal oxide with a large exciton binding energy of 60 meV, which makes it a promising material for optoelectronic applications. It has attracted increasing attention

and stimulated intense research efforts since theoretical calculations predict Mn-doped ZnO can show ferromagnetism with a T_c value above room temperature making it a promising candidate for spintronic applications too. ZnO crystallizes in the wurtzite structure with tetrahedral sp^3 bonding. When doped with Mn to form $Zn_{1-x}Mn_xO$, Mn atoms substitute the Zn atoms in the crystal lattice. The electronic configuration of Mn is $1s^2, 2s^2, 2p^6, 3s^2, 3p^6, 3d^5, 4s^2$ and during substitution, Mn donates its $4s^2$ electrons to the sp^3 bonding and exists as Mn^{2+} ions. The half filled 3d band of Mn^{2+} has 5 electrons and it hybridizes with the p-bands of oxygen in ZnO. This results in an exchange interaction between the localized magnetic moments (3d spins) and the spins of itinerant carriers in the host ZnO. Several mechanisms have been proposed to explain ferromagnetism in DMS. These include the Zener model [18], carrier mediated exchange [3], double exchange [5, 19] and coupling via a bound magnetic polaron [20, 21].

According to the Zener model, since the Mn-d shell is only half filled, the direct interaction between d shells of adjacent Mn atoms leads to an antiferromagnetic state. However, the indirect coupling of spins through itinerant carriers tends to align the spins of the d shell electrons in a ferromagnetic manner. Ferromagnetism is therefore assumed to occur due to interactions between the local moments of the Mn atoms, mediated by free holes in the material. Based on this model, TM-doped p-type ZnO is predicted to be a promising candidates for ferromagnetic DMS with high Curie temperature. However, these predictions are based on the incorporation of $\approx$ 5% TM element into the host and hole concentrations of above $10^{20} cm^{-3}$. Considering that p-type doping has always been a challenge in II-VI semiconductors, the achievement of such high hole concentrations is not realistic.

The Zener double exchange was used to explain ferromagnetism in TM doped InAs [19] and is an indirect coupling mechanism between two neighboring TM ions. According to this theory, if neighboring TM magnetic moments are in the same direction, there is a widening of the TM-d band due to hybridization of the spin states. The band energy of the ferromagnetic state can be lowered below that of the antiferromagnetic state if a sufficient number of holes (or electrons) exist. The 3d electrons of the TM ions hop to the 3d orbitals of neighboring TM ions with parallel magnetic moments, thus lowering its energy by hopping in the ferromagnetic state.

In all of the proposed mechanisms, the impact of charge state and the involved electronic 3d-shell configuration of TM ions are crucial points in understanding the magnetic mechanism within the diluted magnetic semiconductors. Experimental investigations have shown that Mn-substituted ZnO samples exhibit distinct magnetic properties including spin-glass behavior [22]; paramagnetism [23]; ferromagnetism with T_c of 45 K [24]; ferromagnetism with T_c of 425 K in thin films of Mn doped ZnO [2] and $T_c > 400$ K for Mn doped ZnO nanowires [7]. Structural defects have also been reported to play an important role in the occurrence and stability of ferromagnetism [25]. To interpret the origin of the magnetic properties, many magnetic interaction mechanisms have been proposed, including direct super-exchange, indirect superexchange, and carrier-mediated exchange. In spite of all these works, the local structure and microscopic origins of the high-T_c ferromagnetism in ZnO, GaN, and Si-based DMSs are still under debate. This debate has emerged as one of the most important challenges in understanding the science of DMS.

3. Ferromagnetic II-VI nanowires

The attractive features in using II-VI semiconductors for fabricating DMS are several: interesting opto-electronic properties, high solubility of transition metal atoms in the host lattice (implies that the amount of injected spins can be large), and also because II-VI materials like ZnO are cheap, abundant in nature and are also environmentally friendly. The ternary nature of the $A^{II}_{1-x}Mn_xB^{VI}$ alloys, allows the possibility of 'tuning' the lattice constant and band parameters by varying the composition of the material. The substitutional Mn atoms in the $A^{II}B^{VI}$ lattice are also characterized by highly efficient electroluminescence, which makes dilute $A^{II}_{1-x}Mn_xB^{VI}$ alloys important in optical flat panel display applications. However, since Mn atoms do not provide any carriers when they are substituted in the insulating host $A^{II}_{1-x}Mn_xB^{VI}$ lattice, it was believed for a long time that the magnetic interaction in II-VI DMS is dominated by antiferromagnetic exchange among the Mn spins, which would result in paramagnetic or antiferromagnetic behavior of the material. The prediction of room temperature ferromagnetism in TM doped II-VI semiconductors initiated intense theoretical and experimental work on II-VI materials, with several contradicting results. Of the II-VI semiconductors, ZnO is particularly interesting because it has a smaller lattice constant compared to other IIŰVI semiconductors, which will serve to increase the magnetic coupling strength among the magnetic ions.

3.1. Synthesis and structural characterization of $Zn_{1-x}Mn_xO$ nanowires

The $Zn_{1-x}Mn_xO$ nanowires were grown on Si substrates by the vapor phase growth, using the VLS mechanism [7]. The growth temperature was $700^{\circ}C$. Mn doping was achieved by using MnO_2 as the dopant material, which was evaporated at $700^{\circ}C$. A mixture of ZnO and graphite was used as the source material, evaporated at $900^{\circ}C$. After growth for an hour, the Si surface was found coated with a grayish colored substance. The morphologies of this product was investigated by a scanning electron microscope (SEM) using Hitachi SEM S-5200, and a high resolution transmission electron microscope (HRTEM) using Hitachi STEM HD-2000. Magnetic properties of these samples were studied by superconducting quantum interference device (SQUID) magnetometer (MPMS MultiVu Application). The Mn content was determined by Energy Dispersive X-ray (EDX) spectroscopy and Ion Coupled Plasma Mass Spectrometry (ICPMS) using Perkin Elmer Sciex ELAN DRC II. The morphology of the $Zn_{1-x}Mn_xO$ nanowires was observed using SEM, which revealed that the nanowires have lengths in the range of 8–10 μm and diameter between 40–150 nm. The crystallinity of the $Zn_{1-x}Mn_xO$ nanowires as evidenced by HRTEM is shown in Figure 2. The image clearly reveals the lattice fringes of ZnO $\{0001\}$ planes with an interplanar spacing of about 0.52 nm, indicating that the nanowire is a single crystal and grows along the [001] direction, as shown in Figure 2. No observable change in structure was noted between pure and Mn doped nanowires. All the wires were straight and had a smooth surface, which also confirms that Mn is doped into the lattice structure instead of being precipitated as a second phase.

The composition of the nanowires was characterized by EDX at nanometer resolution. All samples show uniform distribution of Zn, O and no other impurities other than Mn (Figure 3. The signal from Si is due to the substrate. Due to the limited sensitivity of EDX at high resolution, Mn atoms were detected only in samples with more than 2% Mn concentration although ferromagnetism was observed in all Mn-doped samples as discussed below. The elemental mapping (EDX) spectra show a highly uniform distribution of Mn atoms with

http://dx.doi.org/10.5772/52825

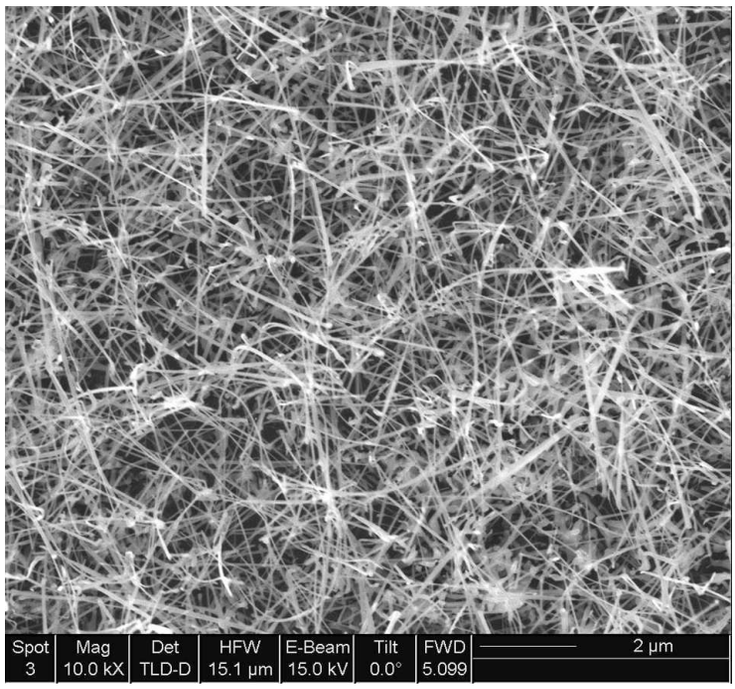

Figure 1. SEM image of $Zn_{1-x}Mn_xO$ nanowires growing in a 'weed-like' manner on Si substrate.

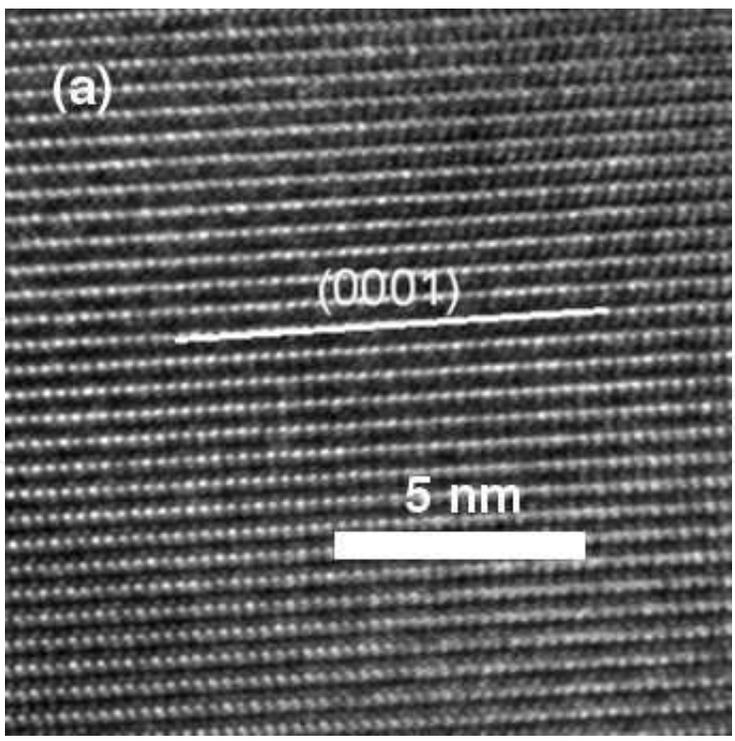

Figure 2. HRTEM image of a crystalline $Zn_{1-x}Mn_xO$ nanowire. The nanowire has smooth surface and there is no evidence of any secondary phases or defects on these nanowires.

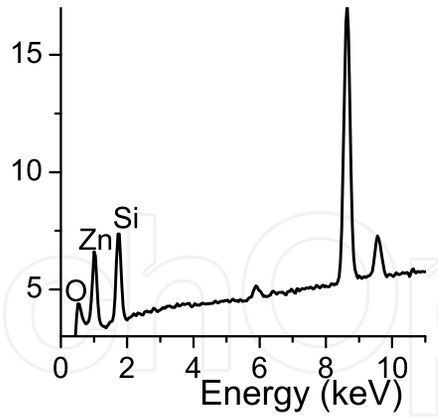

Figure 3. EDX spectra for $Zn_{1-x}Mn_xO$ nanowires, with ~ 2 $at\%$ Mn.

no clustering or segregated Mn-rich phases. As the growth method does not allow us to precisely control the Mn concentration and the sensitivity of EDX is limited, ICPMS (a destructive chemical analysis method) was done to estimate the Mn concentration. The nanowires were first dissolved in HNO_3 and subsequently introduced into an extremely hot (7,000 to 10,000 K) radio frequency induced argon plasma. The plume of the argon plasma is sampled directly into the entrance orifice of a quadrupole mass spectrometer. Analyte ions produced by the plasma are accelerated, magnetically separated and counted using an electron multiplier. In all samples the Mn concentration was measured to be in the range of 1% to 4%.

3.1.1. SQUID measurements of magnetization on $Zn_{1-x}Mn_xO$ nanowires

Magnetization measurements, using a SQUID magnetometer (MPMS MultiVu Application) showed a distinct hysteresis loop superimposed on a diamagnetic contribution from the substrate (Figure 4).

Figure 5 shows the variation of magnetization (M) with temperature T, measured during cooling in an applied magnetic field of 100 Oe. The magnetization decays very slowly with T over the range studied. T_c is well above room temperature, but it is hard to determine the exact value, since the value of T_c is rather high, exceeding the range of measurements. The same conclusion can be reached from the dependence of remnant magnetization (M_r) and coercive field (H_c) on temperature (Figure 5). M_r and H_c are 2.44×10^{-6} e.m.u and 37.05 Oe respectively at 300 K.

3.1.2. Estimation of magnetic moment per Mn atom in $Zn_{1-x}Mn_xO$ nanowires

The $Zn_{1-x}Mn_xO$ nanowires were grown on Si substrates of area 9 mm^2. The nanowires had an average length of 10 μm and hence the maximum volume of nanowires is estimated to be 9×10^{-5} cm^3. For Mn concentration varying from 1 $at\%$ to 4 $at\%$, the number of Mn atoms (N_{Mn}) is estimated to vary from $2 \pm 0.8 \times 10^{15}$ $atoms/cm^3$ to $8 \pm 3.2 \times 10^{15}$ $atoms/cm^3$. The magnetic moment per Mn atom (in terms of the Bohr magneton) was determined by the equation:

http://dx.doi.org/10.5772/52825

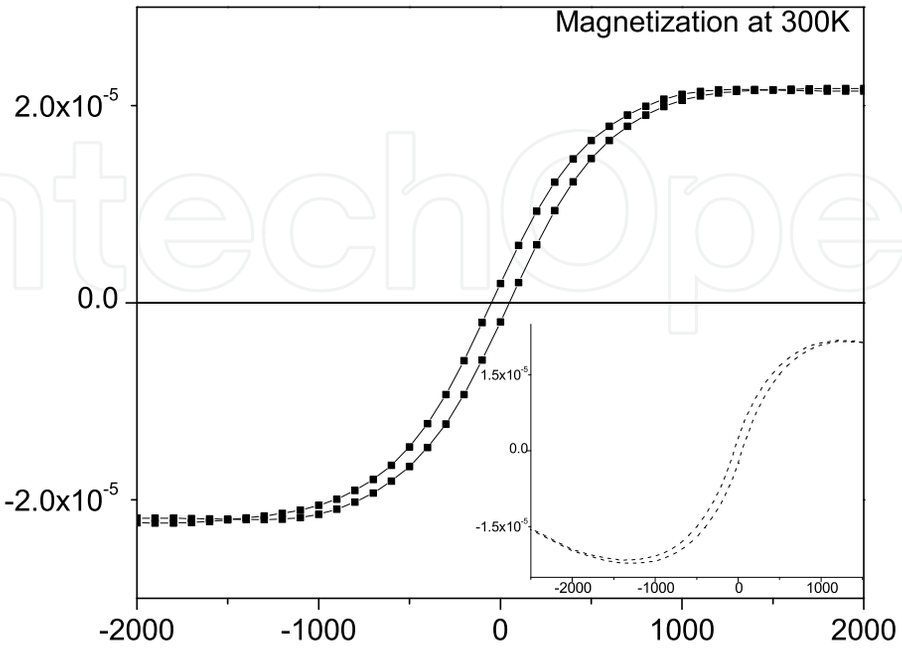

Figure 4. Hysteresis loop (M-H curve) of $Zn_{1-x}Mn_xO$ nanowires at a temperature of 300 K; inset: the as-obtained data from the SQUID measurements including the diamagnetic contribution arising from the Si substrate.

$$\frac{m}{\mu_B} = \frac{M_s}{N_{Mn}(9.27 \times 10^{-24})} \tag{1}$$

where M_s is the saturation magnetization. From the observed saturation magnetization (Figure 4), M_s is of the order of $2.0 - 3.0 \times 10^{-5}$ e.m.u $(2.0 - 3.0 \times 10^{-8}\ A.m^2)$, and the magnetic moment per Mn atom is estimated to be in the range of 0.30 μ_B to 1.2 μ_B, which is smaller than the maximum spin moment (5 μ_B) per Mn^{2+} with S = 5/2 and g=2; but is larger than those reported in previous reports [2].

3.1.3. Optical characterization of Mn doped and undoped ZnO nanowires

The luminescence spectra of ZnO exhibits strong mid-gap green emission, which has been occasionally attributed to Zn interstitials [26] and Zn vacancies [27], the most widely accepted origin of this emission is oxygen vacancies [28, 29]. The $Zn_{1-x}Mn_xO$ and undoped ZnO nanowires were characterized by room temperature photoluminescence (PL) measurements.

The wires were excited by a 355 nm wavelength laser at room temperature. The photoluminescence spectrum shown in Figure 6 shows a very weak band edge luminescence from exciton (UV emission) at about 380 nm and a strong mid-gap emission (green emission) at about 525 nm. The ZnO band edge emission is extremely weak possibly because of strong

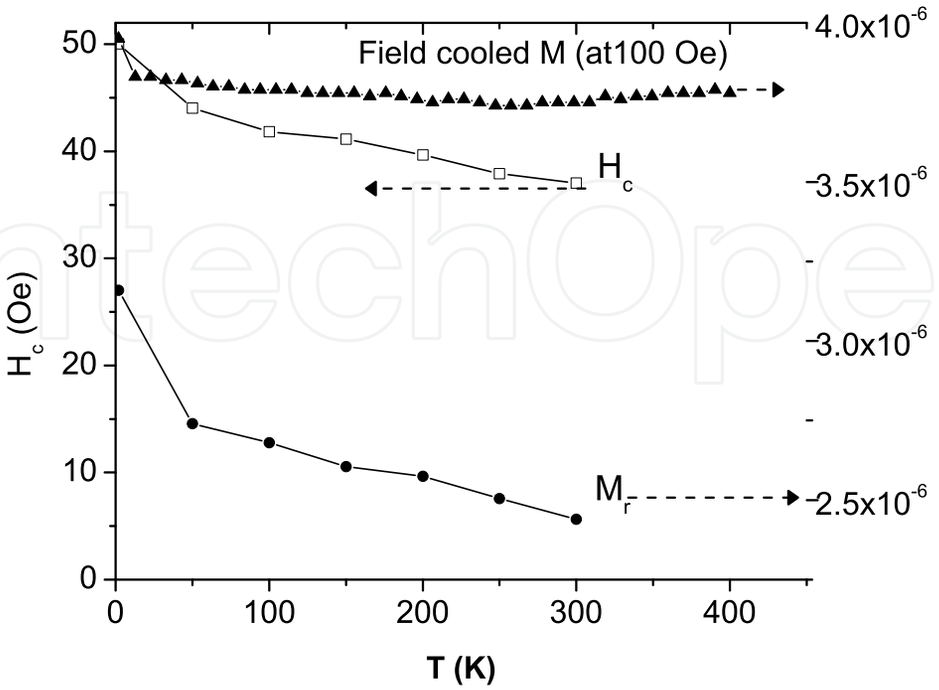

Figure 5. Dependence of remnant magnetization (M_r), coercive field (H_c) and field cooled magnetization (M-T at 100 Oe) of $Zn_{1-x}Mn_xO$ nanowires on temperature.

non-radiative processes due to the large density of surface states in a nanowire. When doped with Mn, a strong suppression of the mid-gap emission is observed followed by a substantial increase in the band-edge luminescence. Although most Mn-doped II-VI materials show a manganese specific orange emission no such luminescence was observed in Mn doped ZnO nanowires. This is consistent with previous reports on Mn-doped ZnO [30, 31], but the reason for this absence of Mn-related emission is not clear. Although, the strong suppression of the oxygen vacancy related emission could be due to Forester type dipole-dipole energy transfer, the small oscillator strength of Mn absorption would make such a process very inefficient. The suppression of mid-gap emission in Mn-doped II-VI materials implies a more efficient direct capture of photo excited carriers before getting trapped by states responsible for mid-gap emission. However, such a process would lead to suppression of band-edge luminescence as well, contrary to the observation of enhanced band-edge emission. These results therefore indicate that there is an interaction between Mn doping and native defects like oxygen vacancies. The mechanism of such an interaction is not clear and deserves further study.

3.1.4. Discussion

Unlike previous reports, the observed ferromagnetism can be attributed only to the Mn doped into the ZnO lattice structure since HRTEM revealed a clean and smooth surface of the nanowire and no precipitates or attachments to the wire surface were observed. No ferromagnetic behaviour was observed for pure ZnO nanowires. Moreover, ferromagnetic impurity phases responsible for the observed magnetic ordering can be ruled out since there

http://dx.doi.org/10.5772/52825

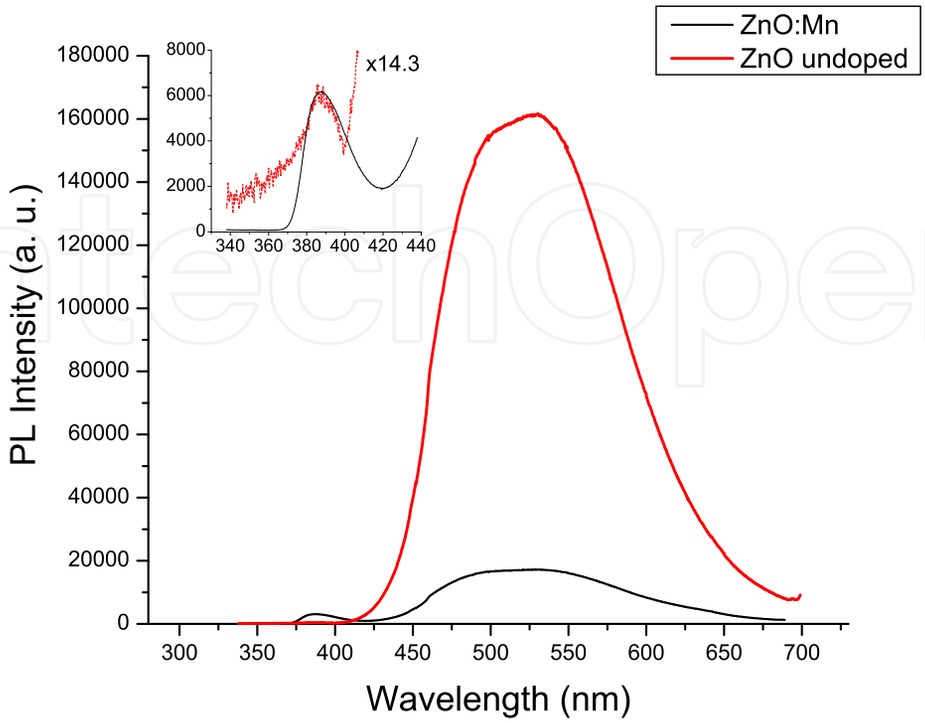

Figure 6. Room temperature photoluminescence spectra of undoped and $Zn_{1-x}Mn_xO$ nanowires.

is no known phase of manganese oxide with above room temperature T_c. All the possible MnO_x phases that could be forming in our growth process are antiferromagnetic, with the exception of Mn_3O_4, which is ferromagnetic below 45 K. In contrast to the bulk and thin film samples studied in the past we have single crystal nanowires and no evidence for multiple phases. The nanowires studied here are not intentionally doped. In general, undoped ZnO tends to be n-type due to intrinsic defects. Although the large density of surface states and the VLS mechanism of nanowire growth can potentially make them p-type, we do not have any evidence for substantial hole concentration in these samples. In order to estimate the conductivity of the nanowire array, a sample for conductivity measurements was prepared following the procedure described in Reference [32]. Conductivity measurements on ZnO nanowire arrays show that these wires are conducting but the observed resistance is more than 1 GΩ per wire implying very low mobile carrier concentration. However, carrier mediated exchange interaction only requires itinerant carriers that hybridize with the Mn 3-d band so that hopping of localized spins between Mn ions can stabilize the parallel spin configuration. The material may still remain semi-insulating or show hopping conductivity [33]. Further, conduction through nanowires are known to be very sensitive to charge inhomogeneities along the length of the wire [32]. Even though ferromagnetism is predicted and expected in p-type Mn doped ZnO through strong p-d hybridization [3], Sato et al. [5] predicted that the ferromagnetic state of Co^{2+}(d7) in Co-doped ZnO can be stabilized by $s-d$ hybridization, thus making it possible to obtain high Curie temperature ferromagnetic materials in n-type ZnO.

3.2. Synthesis and characterization of $Zn_{1-x}Fe_xO$ nanotubes

Sato et al.,[34] used first principles calculations to predict that the ferromagnetic state is stable in V-, Cr-, Fe-, Co- or Ni-doped ZnO without any additional carrier doping treatments. It is believed that (Zn,Fe)O is a promising candidates for high T_c ferromagnets, and there are reports of ferromagnetism in Fe-doped ZnO nanocrystals [35], and with co-doping [36, 37]. In this section, a recent work in the author's research group[38] on the synthesis of $Zn_{1-x}Fe_xO$ nanotubes with clear evidence of Fe ions substituting for Zn^{2+} ions in the ZnO crystal lattice is presented. The Fe-doped ZnO nanotubes were synthesized by a simple electrochemical process at $75^{\circ}C$ using $ZnCl_2$ and KCl mixed with Fe as an electrolyte. The undoped ZnO compound has near-zero or negligible magnetic moment, since all its electrons are paired. However, when ZnO is doped with Fe (which has an incomplete d subshell), it exhibits a magnetic moment that is determined by the number of unpaired electrons in the doped compound. The determination of the magnetic moment was done using a technique similar to the Gouy method [39]. In this technique, an Evans balance was employed to measure the change in current required to balance suspended magnets when their magnetic field interacts with a magnetic sample. This value was then used to determine the effective magnetic moment. Magnetization measurements on the $Zn_{1-x}Fe_xO$ nanotubes have not been completed and so no claims can be made on the ferromagnetic property of these nanostructures.

Synthesis of ZnO nanotubes was done in a three electrode standard electrochemical cell with a Si(111) substrate coated with 300 nm Au film as the cathode and the working electrode. The counter electrode was made of Pt. The electrolyte comprised of a mixture of $FeCl_3$ (0.1 mM) + $ZnCl_2$ (6 mM) + KCl (0.2 M)]. Synthesis was carried out in a temperature-controlled water bath maintained at $75^{\circ}C$. Oxygen (20 sccm) was continuously bubbled through the electrolyte during the growth process. A constant bias of -1 V was maintained between the working and reference electrodes during the growth process. Post growth, the nanostructures were characterized by SEM (NOVA dual-beam SEM/FIB, FEI Nova 200 Nano-Lab), HRTEM (FEI Tecnai G2 F20 S-Twin 200 keV), and selected-area electron microscopy (SAED) pattern analysis. Composition and structural analysis were further done by EDX and x-ray diffraction (XRD) (Rigaku Ultima III). The hexagonal ZnO nanotubes had wall thickness of 20 nm and pore diameter in the range of 80 nm to 120 nm, as shown in Figure 7(a) and (b). EDX analysis of the nanotubes showed a Fe peak, confirming a dilute concentration of Fe $(< 4wt.\%)$ in the nanotubes. Electrolyte concentration, growth time, and growth temperature play a vital role in determining the morphology of the nanostructures. The first stage of the synthesis process was the growth of nanorods, which was followed by etching of the nanorods along a specific plane. The etching process was facilitated by the high concentration of KCl in the electrolyte.

3.2.1. XRD measurements on $Zn_{1-x}Fe_xO$ nanotubes

Figure 8 shows results of XRD measurements on undoped and Fe doped ZnO nanotubes. The diffraction peaks have been indexed to the hexagonal ZnO wurtzite structure. The strong peak at $2\theta = 34.36^{o}$ corresponds to the (0002) c-axis of ZnO, which indicates that the nanotubes preferentially grow along (0001) direction. No additional peak attributed to Fe or its oxide could be detected in the XRD spectrum of Fe-doped ZnO nanotubes, though a small shift of the (0002) peak was observed. This shift of the (0002) peak position for

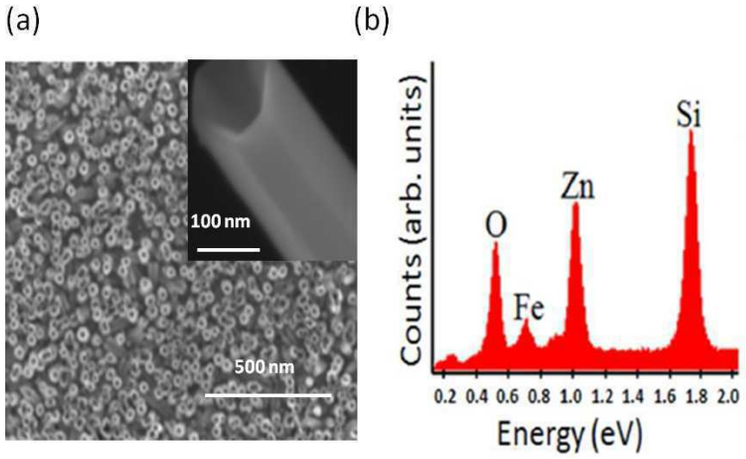

Figure 7. SEM image of nanotubes: (a) $Zn_{1-x}Fe_xO$ nanotubes with wall thickness of about 20 nm and pore diameter of about 80 nm to 120 nm. Inset shows a magnified SEM image of a single Fe-doped ZnO nanotube. (b) EDX spectrum confirming the presence of Fe, Zn, and O. The Fe concentration is estimated to be about 3-4 wt.%.

the Fe-doped ZnO indicates that there is an increase in the c-axis lattice parameter for the Fe-doped sample, indicative of the fact that Fe ions substitute for Zn^{2+} ions in the ZnO lattice, without changing its wurtzite crystal structure. The ionic radius of Fe^{2+} is larger than that of Zn^{2+} by about 5%. Hence, when Fe^{2+} ions occupy the Zn^{2+} sites of ZnO, the in-plane atomic arrangement with closed atomic packing will be strained due to the substitution of Zn by the larger Fe atom. This cause an increase in the c-lattice constant and a shift of the (0002) peak to smaller angle in the XRD pattern of the Fe-doped ZnO nanotubes. It is also possible that Fe^{2+} and Fe^{3+} ions are both present and occur as substitutional as well as interstitial dopants. In this case, the atomic arrangement is disturbed and the number of interstitials will increase, which will result in lattice disorder and strain. A comparison of the XRD spectrum of the undoped and doped nanotubes (inset of Figure 8) shows that the full-width at half maximum (FWHM) of the (002) diffraction peak is broadened (about 3% to 4%) and its intensity decreased in the Fe-doped ZnO nanotubes. This indicates that the dilute (<4 wt.%) Fe doping influences the crystalline quality of the nanotubes by causing lattice defects. This result was further validated by comparison of the PL spectra before and after doping.

3.2.2. Optical characterization of $Zn_{1-x}Fe_xO$ nanotubes

The nanostructures were optically characterized by photoluminescence (PL) spectroscopy and Raman spectroscopy. PL spectra were obtained using a TRIAX 320 spectrometer with excitation provided by a Kimmon continuous-wave HeCd laser with spot size of about 1 mm^2. The Raman spectrum was obtained using an Almega XR 532 nm (green) laser.

Figure 9 shows the room-temperature PL spectra for the undoped and Fe-doped ZnO nanotubes. The curves with solid lines and symbols represent the experimentally obtained data for the undoped and Fe-doped ZnO nanotubes.

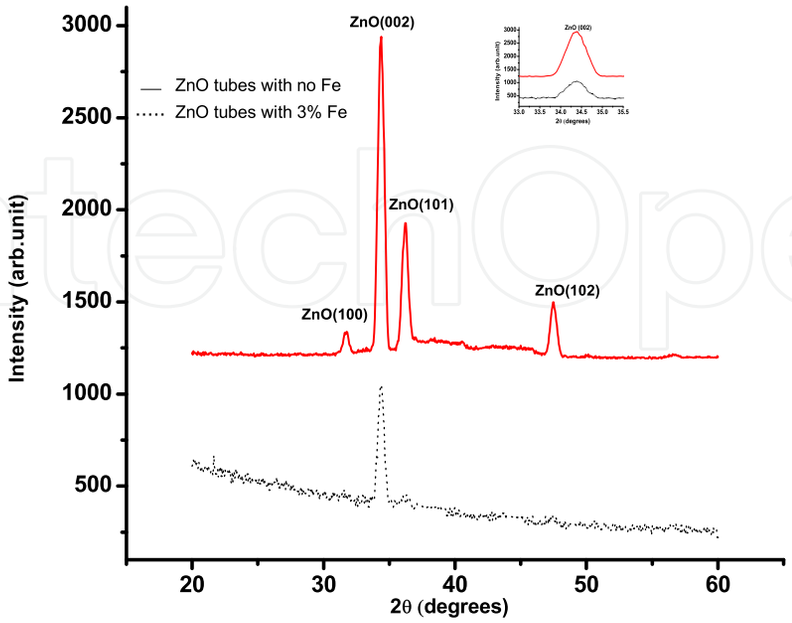

Figure 8. XRD spectrum of undoped (solid line) and Fe-doped (dotted line) ZnO nanotubes. Inset shows the broadening of (0002) peak for Fe-doped nanotubes.

The broad defect peak in the Fe-doped sample was de-convoluted using a Gaussian distribution (shown by dashed curves). The PL spectra for undoped ZnO tubes showed strong band-edge emission at 370.5 nm (3.35 eV) and no other peaks, attesting to the high crystalline quality of the undoped nanotubes. However, when doped with Fe, the PL spectrum showed an ultraviolet (UV) emission peak at $\approx 381nm$ (red-shifted) and a

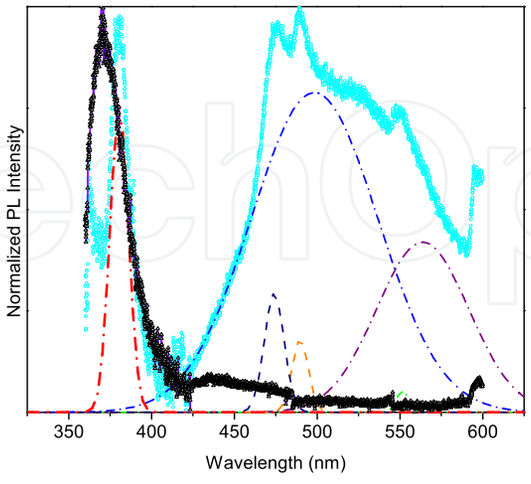

Figure 9. Room-temperature PL spectra of undoped and Fe-doped ZnO nanotubes. The normalized curves with solid lines and symbols represent the experimentally obtained data. The curves shown by dotted lines represent the Gaussian fit of PL spectra for Fe-doped nanotubes.

broad emission peak in the visible region. The red-shift of the band edge in Fe-doped II-VI semiconductors has been attributed to the $sp-d$ spin exchange interactions between the band electrons of the host and localized d electrons of the Fe ion substituting the group II ion [40]. A Fe^{2+} cation is in $3d^6$ configuration. The sŰp and pŰd exchange interactions between ZnO as host and Fe as dopant give rise to a negative and positive correction to the conduction- and valence-band edges, leading to narrowing of the band gap. Thus, the red-shift and quenching of the UV emission peak in the doped sample provide further evidence of the fact that Fe substitutes for Zn in the ZnO crystal [41]. The broad defect-related emission peak was deconvoluted into Gaussian peaks at 474 nm, 489 nm, 499 nm, 551 nm, and 563 nm. The peak observed at 474 nm is attributed to interstitial Zn and oxygen. The peaks at 489 nm and 499 nm are attributed to singly ionized oxygen vacancies, whereas the peaks at 551 nm and 563 nm are attributed to oxygen interstitials.

Figure 10(a) and (b) compare the Raman spectrum for the undoped and Fe-doped ZnO nanotubes. Both samples show a Raman shift at 521 cm^{-1} corresponding to the Si substrate used for the growth of ZnO nanotubes. The undoped sample shows a characteristic Raman peak at 438 cm^{-1}, related to the hexagonal wurtzite phase of ZnO. The Fe-doped sample shows additional peaks at 336 cm^{-1}, 384 cm^{-1}, and 644 cm^{-1}.

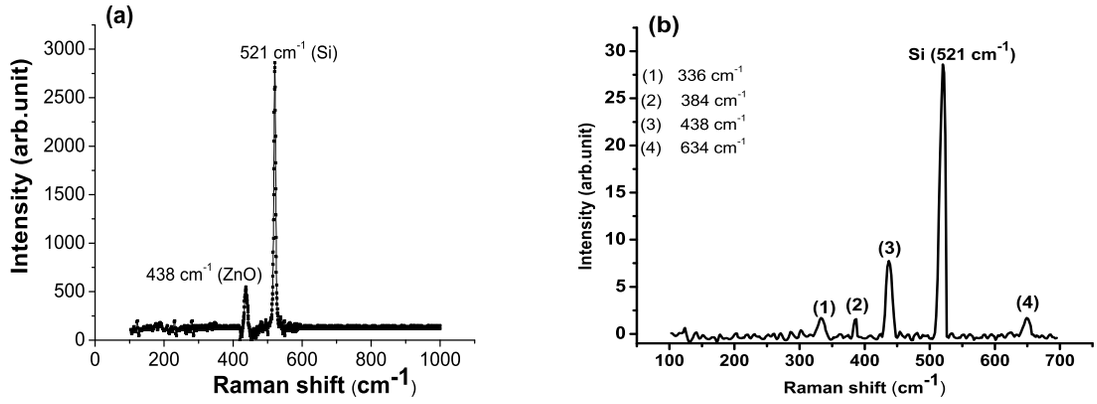

Figure 10. Raman scattering spectrum for: (a) undoped ZnO nanotubes and (b) Fe-doped ZnO nanotubes

The peaks at 336 cm^{-1} and 384 cm^{-1} are attributed to intrinsic defects in ZnO such as oxygen vacancies and zinc interstitials. The additional vibrational mode at 644 cm^{-1} in the Fe-doped ZnO nanotubes is also related to intrinsic ZnO lattice defects, which either become activated as vibrating complexes upon addition of Fe, or their concentration increases upon Fe incorporation into the ZnO lattice.

3.2.3. Determination of effective magnetic moment in $Zn_{1-x}Fe_xO$ nanotubes

Further evidence of the successful incorporation of Fe into ZnO was obtained through determination of the effective magnetic moment (μ_{eff}) for the undoped and Fe-doped ZnO nanotubes. This was done using a magnetic susceptibility balance (Evans balance), which measures the force experienced by a substance when it is placed in a magnetic field. The nanotubes were placed in a cylindrical tube, which was placed in a uniform magnetic field.

The effective magnetic moment was measured in units of Bohr magnetron (μ_B)using the equation:

$$\mu_{eff} = 2.828(\chi_A T)^{1/2} \tag{2}$$

where χ_A is the corrected molar susceptibility of the sample at temperature T (room temperature). χ_A for $Zn_{1-x}Fe_xO$ and undoped ZnO nanotubes was determined to be $\approx 1.31 \times 10^{-2}$ cgs units and $\approx 1.68 \times 10^{-4}$cgs units respectively. The effective magnetic moment was then calculated for both samples and found to be $\approx 5.41\mu_B$ for Fe-doped and $\approx 0.62\mu_B$ for undoped ZnO nanotubes. These values of μ_{eff} correspond to four unpaired electrons in the $Zn_{1-x}Fe_xO$ nanotubes and zero unpaired electrons in the undoped ZnO nanotubes. The four unpaired electrons found in the Fe-doped material is consistent with the electron configuration of Fe^{2+} in a high spin tetrahedral geometry, and is expected from the incorporation of Fe^{2+} as a substitutional dopant in ZnO. The undoped ZnO nanotubes showed a near zero effective magnetic moment.

4. Conclusion

There are several works in favor of and against ferromagnetism in TM doped ZnO. Experimentalists have frequently observed ferromagnetism in this material though the theory to support this claim does not exist. The promise of obtaining materials with high Curie temperature and thus develop spin-based semiconductor devices keeps the field of II-VI DMS very active. The electronic properties of nanoscale DMS are strongly affected by quantum confinement effect and large surface to volume ratios; hence the magnetic coupling between TM ions in low-dimensional systems may be distinctively different from that of bulk materials. Ferromagnetism in Mn-doped ZnO nanowires is yet to be understood, as Mn in its +2 valence state is an isovalent dopant and does not provide any carrier to ZnO. Hence, by first-principles studies, it must lead to an antiferromagnetic ground state. However, experimental observation of room temperature ferromagnetism in Mn-doped ZnO thin films and nanostructures have posed a challenge to the theoretical understanding of ferromagnetism for such systems. To complicate matters further, recent experiments reveal inconsistent ferromagnetic properties for TM doped ZnO, leaving the real mechanism for ferromagnetism in ZnO unclear. Experimental studies have revealed the importance of defects such as zinc and oxygen interstitials and vacancies on the magnetic ordering in such systems. It is evident that the observed ferromagnetic ordering as well as the measured magnetic moment and T_c depends largely on sample preparation techniques. Even in low dimensional systems, there could be several ferromagnetic sources, such as (a) contaminated substrate, (b) clusters of intrinsic defects with ferromagnetically aligned spins, (c) clusters of TM ions, and (d) uncompensated surface spins.

The first step in the synthesis of DMS is the successful incorporation of the TM ion into the host (ZnO) lattice. In this regard, we present our recent work on the synthesis of $Zn_{1-x}Fe_xO$ nanotubes with clear evidence of Fe ions substituting for Zn as 2+ ions in the ZnO crystal lattice. Nanotubes are interesting since the pores in them provide an additional dimension for band gap engineering and tuning of properties.

There is no clear understanding on the origin of ferromagnetism in low dimensional II-VI systems such as ZnO when doped with TM ions. There are several important issues that need to be resolved. It needs to be ascertained if the existence of room temperature ferromagnetism is related to some intrinsic origin and not to the presence of defects. If defect induced ferromagnetism is implicated, then the application of this DMS becomes very limited.

Author details

Usha Philipose and Gopal Sapkota

Department of Physics, University of North Texas, USA

References

[1] H. Ohno(2001). Toward Functional Spintronics. *Science*, Vol.291[5505]: 840-841

[2] P. Sharma et al.,(2003). Ferromagnetism above room temperature in bulk and transparent thin films of Mn doped ZnO. *Nature Materials*, Vol.2: 673-677

[3] T. Dietl,H. Ohno,F. Matsukura,J. Cibert,D. Ferrand (2000). Zener model description of ferromagnetism in zinc-blende magnetic semiconductors. *Science*, Vol.287[5455]: 1019-1022

[4] K. Sato and H. Katayama-Yoshida (2000). Material design for transparent ferromagnets with ZnO-based magnetic semiconductors. *Japanese Journal Of Applied Physics*, Vol.39[6B]: L555-558

[5] K. Sato and H. Katayama-Yoshida (2001). Stabilization of ferromagnetic states by electron doping in Fe-, Co- or Ni-doped ZnO. *Japanese Journal Of Applied Physics*, Vol.40:L334-336

[6] T. Jungwirth et al.,(2005). Prospects for high temperature ferromagnetism in (Ga,Mn)As semiconductors. *Physical Review B*, Vol.72[16]: 165204:1-13

[7] U. Philipose, Selvakumar V. Nair, Simon Trudel, C. F. de Souza, S. Aouba, Ross H. Hill, Harry E. Ruda (2006). High temperature ferromagnetism in Mn doped ZnO nanowires. *Applied Physics Letters*, Vol.88[26]: 263101:1-3

[8] Z. H. Zhang, X. Wang, J. B. Xu, S. Muller, C. Ronning and Quan Li (2009). Evidence of intrinsic ferromagnetism in individual dilute magnetic semiconducting nanostructures. *Nature Nanotechnology*, Vol.4: 523-527

[9] C. Liu, F. Yun and H. Morkoc (2005). Ferromagnetism of ZnO and GaN: A review. *Journal of Materials Science: Materials in Electronics*, Vol.16: 555-597

[10] S.J. Pearton, W.H. Heo, M. Ivill, D.P. Norton and T. Steiner (2004). Dilute magnetic semiconducting oxides. *Semiconductor Science and Technology*, Vol.19[10]: R59-74

[11] F. Pan, C. Song, X. J. Liu, Y. C. Yang and F. Zeng (2008). Ferromagnetism and possible application in spintronics of transition-metal-doped ZnO films. *Materials Science and Engineering: R: Reports*, Vol.62[1]: 1-35

[12] S.J. Pearton et al., (2007). Ferromagnetism in transition-metal doped ZnO. *Journal of Electronic Materials*, Vol.36[4]: 462-471

[13] S. J. Han, T. H. Jang, Y. B. Kim, B. G. Park, J. H. Park and Y. H. Jeong (2003). Magnetism in Mn-doped ZnO bulk samples prepared by solid state reaction. *Applied Physics Letters*, Vol.83[5]: 920-922

[14] S. Kolesnik and B. Dabrowski (2004). Absence of room temperature ferromagnetism in bulk Mn-doped ZnO. *Journal of Applied Physics*, Vol.96[9]: 5379-5381

[15] H. S. Hsu et al.,(2006). Evidence of oxygen vacancy enhanced room-temperature ferromagnetism in Co-doped ZnO. *Applied Physics Letters*, Vol.88[24]: 242507:1-3

[16] K. R. Kittilstved, D. A. Schwartz, A. C. Tuan, S. M. Heald, S. A. Chambers and D. R. Gamelin (2001). Direct Kinetic Correlation of Carriers and Ferromagnetism in Co^{2+} : Zn. *Physical Review Letters*, Vol.97[3]: 037203:1-4

[17] H. S. Hsu, et al.,(2008). Magnetic coupling properties of Mn-doped ZnO nanowires: First-principles calculations. *Journal of Applied Physics*, Vol.103[7]: 073903:1-5

[18] C. Zener (1951). Interaction Between the d Shells in the Transition Metals. *Physical Review B*, Vol.81[3]: 440-444

[19] H. Akai (1998). Ferromagnetism and Its Stability in the Diluted Magnetic Semiconductor (In, Mn)As. *Physical Review Letters*, Vol.81[14]: 3002-3005

[20] J.M.D Coey, M. Venkatesan and C.B Fitzgerald (2005). Donor impurity band exchange in dilute ferromagnetic oxides. *Nature Materials*, Vol.4: 173-179

[21] M. Herbich, A. Twardowski, D. Scalbert and A. Petrou (1998). Bound magnetic polaron in Cr-based diluted magnetic semiconductors. *Physical Review B*, Vol.58[11]: 7024-7034

[22] T. Fukumura et al., (2001). Magnetic properties of Mn-doped ZnO. *Applied Physics Letters*, Vol.78[7]: 958-960

[23] A. Tiwari, C. Jin, A. Kvit, D. Kumar, J.F Muth and J. Narayan (2002). Structural, optical and magnetic properties of diluted magnetic semiconducting $Zn_{1-x}Mn_xO$ films. *Solid State Communications*, Vol.121[6]: 371-373

[24] S.W Jung, S.J An, G. Yi, C.U Jung, S. Lee and S. Cho (2002). Ferromagnetic properties of $Zn_{1-x}Mn_xO$ epitaxial thin films. *Applied Physics Letters*, Vol.80[24]: 4561-4563

[25] K.R Kittilstved, W.K Liu and D.R Gameln (2006). Electronic structure origins of polarity-dependent high T_C ferromagnetism in oxide-diluted magnetic semiconductors. *Nature Materials*, Vol.5: 291-297

[26] L. V. Korsunska et al., (2003). The influence of defect drift in external electric field on green luminescence of ZnO single crystals. *Journal of Luminescence*, Vol.102-103: 733-736

[27] A. F. Kohan, G. Ceder, D. Morgan and C.G. Van de Walle (2000). First-principles study of native point defects in ZnO. *Physical Review B*, Vol.61[22]: 15019-15027

[28] N.E. Hsu, W.K. Hung and Y.F. Chena (2004). Origin of defect emission identified by polarized luminescence from aligned ZnO nanorods. *Journal of Applied Physics*, Vol.96[8]: 4671-4673

[29] F. H. Leiter, H. R. Alves, A. Hofstaetter, D. M. Hofmann and B. K. Meyer (2001). The Oxygen Vacancy as the Origin of a Green Emission in Undoped ZnO. *Physica Status Solidi (b)*, Vol.226[1]: 073903:1-5

[30] X. T. Zhang, Y. C. Liu, J. Y. Zhang, Y. M. Lu, D. Z. Shen, X. W. Fan and X. G. Kong (2003). Structure and photoluminescence of Mn-passivated nanocrystalline ZnO thin film. *Journal of Crystal Growth*, Vol.254: 80-85

[31] M. Liu, A. H. Kitai and P. Mascher (1992). Point defects and luminescence centres in zinc oxide and zinc oxide doped with manganese. *Journal of Luminescence*, Vol.54[1]: 35-42

[32] U. Philipose, H. E. Ruda, A. Shik, C. F. de Souza and P. Sun (2006). Conductivity and photoconductivity in undoped ZnSe nanowire array. *Journal of Applied Physics*, Vol.99: 066106:1-3

[33] Y-J. Ma, Z. Zhang, F. Zhou, Li Lu, A. Jin and C. Gu (2005). Hopping conduction in single ZnO nanowires. *Nanotechnology*, Vol.16[6]: 746-749

[34] K. Sato and H. Katayama-Yoshida (2001). Electronic structure and ferromagnetism of transition-metal-impurity-doped zinc oxide. *Physica B*, Vol.308-310: 904-907

[35] D. Karmakar, S. K. Mandal, R. M. Kadam, P. L. Paulose, A. K. Rajarajan, T. K. Nath, A. K. Das, I. Dasgupta and G. P. Das (2007). Ferromagnetism in Fe-doped ZnO nanocrystals: Experiment and theory. *Physical Review B*, Vol. 75[14]: 144404:1-14

[36] S. W. Yoon et al., (2003). Magnetic properties of ZnO-based diluted magnetic semiconductors. *Journal of Applied Physics*, Vol.93[10]: 7879-7881

[37] M. S. Park and B. I. Min (2003). Ferromagnetism in ZnO codoped with transition metals: $Zn_{1-x}(FeCo)_xO$ and $Zn_{1-x}(FeCu)_xO$. *Physical Review B*, Vol.68[22]: 224436:1-6

[38] G. Sapkota, K. Gryczynski, R. McDougald, A. Neogi and U. Philipose (2012). Low-Temperature Synthesis of Fe-Doped ZnO Nanotubes. *Journal of Electronic Materials*, Vol.41[8]: 2155-2161

[39] Z. Szafran, R.M. Pike, and M.M. Singh, *Micro-Scale Inorganic Chemistry*, Wiley, ISBN 0-471-61996-5, New York.

[40] K.J. Kim and Y.R (2004). Optical investigation of $Zn_{1-x}Fe_xO$ films grown on Al_2O_3(0001) by radio-frequency sputtering. *Journal of Applied Physics*, Vol.96[8]: 4150-4153

[41] A.J. Chen, X.M. Wu, Z.D. Sha, L.T. Zhuge and Y.D. Meng (2006). Structure and photoluminescence properties of Fe-doped ZnO thin films. *Journal of Physics D: Applied Physics*, Vol.39: 4762-4765

IntechOpen